Nano Research 2016, 9(6): 1543–1560
DOI 10.1007/s12274-016-1034-9
Review Article
ISSN 1998-0124
CN 11-5974/O4

Optoelectronic devices based on two-dimensional transition metal dichalcogenides

He Tian[1], Matthew L. Chin[2], Sina Najmaei[2], Qiushi Guo[3], Fengnian Xia[3], Han Wang[1] (✉), and Madan Dubey[2] (✉)

[1] *Ming Hsieh Department of Electrical Engineering, University of Southern California, Los Angeles, California 90089, USA*
[2] *United States Army Research Laboratory, Maryland 20783-1197, USA*
[3] *Department of Electrical Engineering, Yale University, Connecticut 06511, USA*

Received: 3 October 2015
Revised: 22 January 2016
Accepted: 28 January 2016

KEYWORDS

transition metal dichalcogenides (TMDCs), optoelectronic device, molybdenum disulfide (MoS_2), photodetector, light-emitting diode (LED)

ABSTRACT

In the past few years, two-dimensional (2D) transition metal dichalcogenide (TMDC) materials have attracted increasing attention of the research community, owing to their unique electronic and optical properties, ranging from the valley–spin coupling to the indirect-to-direct bandgap transition when scaling the materials from multi-layer to monolayer. These properties are appealing for the development of novel electronic and optoelectronic devices with important applications in the broad fields of communication, computation, and healthcare. One of the key features of the TMDC family is the indirect-to-direct bandgap transition that occurs when the material thickness decreases from multilayer to monolayer, which is favorable for many photonic applications. TMDCs have also demonstrated unprecedented flexibility and versatility for constructing a wide range of heterostructures with atomic-level control over their layer thickness that is also free of lattice mismatch issues. As a result, layered TMDCs in combination with other 2D materials have the potential for realizing novel high-performance optoelectronic devices over a broad operating spectral range. In this article, we review the recent progress in the synthesis of 2D TMDCs and optoelectronic devices research. We also discuss the challenges facing the scalable applications of the family of 2D materials and provide our perspective on the opportunities offered by these materials for future generations of nanophotonics technology.

1 Introduction

Since the successful isolation of graphene a decade ago, the family of two-dimensional (2D) materials has attracted tremendous interest from the research community [1–4]. Graphene is the first extensively

Address correspondence to Madan Dubey, madan.dubey.civ@mail.mil; Han Wang, han.wang.4@usc.edu

studied 2D material. With its unique band structures in the limit of a 2D quantum confinement, this honeycomb-latticed monolayer of carbon atoms has inspired many interesting applications in nanophotonics [5] and nanoelectronics [6]. The most appealing features of graphene for nanophotonic applications originate from its zero-bandgap nature [7], with linear dispersion near the Dirac point [8]. Owing to its unique band structure and various forms of light–matter interaction [9], graphene offers a highly sensitive response to optical signals in a broad spectral range, from far infrared (IR) to ultraviolet (UV). In the mid- and far-IR range ($\geqslant$5 μm wavelength), the light–graphene interaction can be further enhanced through the excitation of propagating plasmons or localized plasmon resonances. Owing to the controllable Fermi level of graphene [10], such responses can be tuned by electrostatic gating [11], which is a feature not available in traditional metal-based plasmonic devices. On the other hand, the inter-band transition in graphene also allows for the construction of detectors [12] and modulators [13] for many optoelectronic applications within the IR, visible, and ultraviolet spectral bands. However, graphene is not the best candidate for applications that require light generation owing to its short carrier lifetime [14], which originates from its zero-gap nature.

Recently, the research community has witnessed the rise of another family of 2D materials—the single-layer transition metal dichalcogenides (TMDCs) [15], such as molybdenum disulfide (MoS_2) and tungsten diselenide (WSe_2). This rich family of mono-molecular-layer semiconductors can cover the energy range from under 1 eV to well above 2.5 eV [16] and beyond, offering new opportunities for constructing devices that can realize light generation functions, such as light-emitting diodes (LEDs) and lasers. In addition, the valley coherence and valley-selective circular dichroism, observed in various monolayer TMDCs, offer novel physical phenomena that can be explored for novel applications in optical computing and communications. Here, we review the synthesis and nanophotonic applications of 2D TMDC materials.

2 Basic structure of TMDCs

TMDCs are materials with the chemical formula MX_2, where M denotes a transition metal element (such as molybdenum (Mo), tungsten (W), niobium (Nb), rhenium (Re), or Titanium (Ti)) while X is a chalcogen (such as sulfur (S), selenium (Se), or tellurium (Te)). Typically, one layer of TMDCs consists of an X–M–X sandwich structure (Fig. 1(a)). The inter-layer interaction of TMDCs is mediated by the weak van der Waals force, while the in-plane bonding is the strong covalent bond. Thus, bulk TMDCs can be exfoliated down to single- or few-layer nanosheets similar to graphene, significantly extending the arsenal of 2D materials. Additionally, TMDC materials such as ReS_2 and $ReSe_2$ have a unique distorted 1T structure with strongly anisotropic in-plane properties (Fig. 1(b)) [17]. Many TMDCs have sizable bandgaps (1–2 eV), with the bandgap width increasing with decreasing the layer number. Some 2D TMDCs, such as molybdenum- and tungsten-based dichalcogenides, have an indirect bandgap in their multi-layer forms, while they become direct-bandgap semiconductors in their monolayer form [18]. The direct bandgap of monolayer TMDCs leads to efficient light emission from these materials, making them promising for developing optoelectronic devices. As shown in Fig. 1(c), the bulk MoS_2 has the bandgap of 1.2 eV. The bandgaps of a trilayer, bilayer, and monolayer MoS_2, determined by photoluminescence (PL), increase to 1.35, 1.65, and 1.8 eV [19], respectively. The bandgap of other typical TMDCs, such as WSe_2, $MoSe_2$ [20], WS_2 [21], and $ReSe_2$ [22], also increases with decreasing the layer thickness, owing to the quantum confinement of carriers in the direction normal to the 2D plane. With TMDCs included in the 2D material family, 2D materials can now benefit applications in the electromagnetic spectral range from far and mid-IR (by using zero-bandgap graphene) to the near IR and visible range (using the TMDCs) and potentially into the ultraviolet range (using hexagonal boron nitride (h-BN)). The diverse range of electronic band structures in this family also offers a wide spectrum of properties, from conductors, semimetals, and semiconductors, to insulators and superconductors. The structural phase transitions between a semiconducting and a metallic crystal structure can also happen in TMDCs [23]. Most recently, Li et al. proposed a new way to realize phase transition in 2D TMDCs by electrostatic biasing [24].

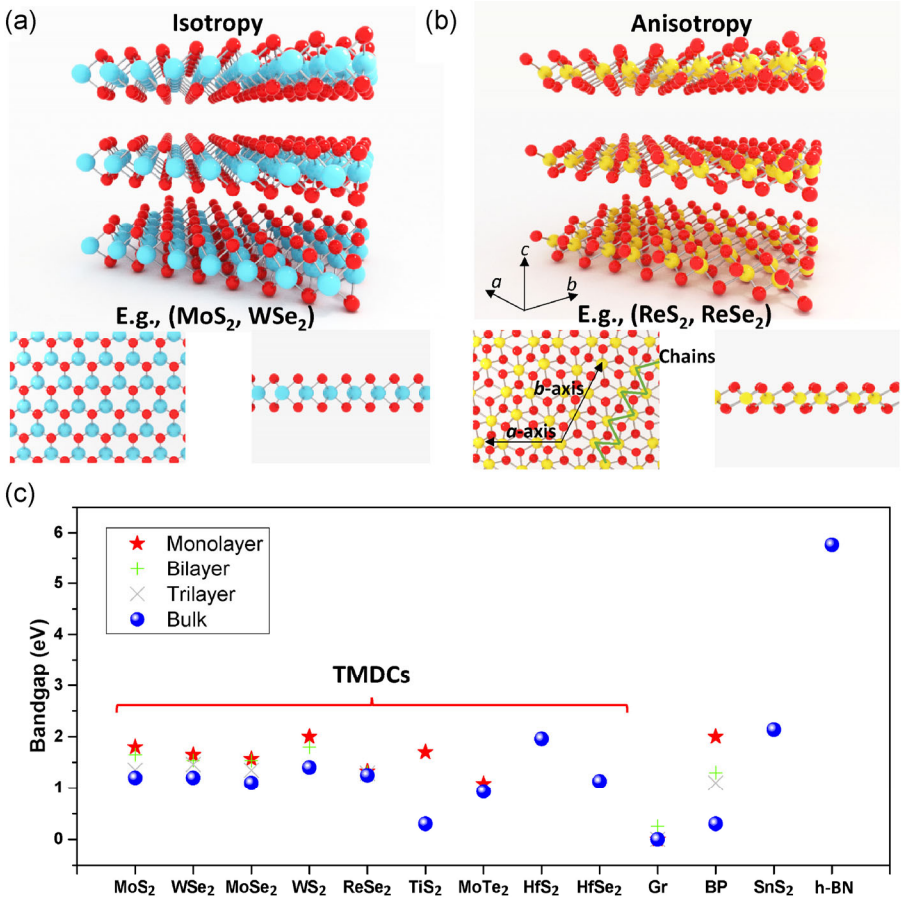

Figure 1 Lattice structure and bandgap of TMDCs. (a) A typical isotropic X–M–X sandwich structure of TMDCs. (b) A typical anisotropic X–M–X sandwich structure of TMDCs. The clustering of M atoms forms the M chains along the lattice vector direction, as shown by the green line. (c) The optical bandgap vs. the layer number for typical TMDCs and other 2D materials (graphene (Gr), black phosphorus (BP), SnS_2, and h-BN). With decreasing the layer number, the bandgap becomes wider. Moreover, the indirect bandgaps of certain bulk TMDCs change into direct bandgaps in their monolayer form.

In addition, exotic optical properties, such as valley coherence and valley-selective circular dichroism [25], have been detected in several common 2D TMDCs including MoS_2 and WSe_2, making these materials attractive for novel optical device applications. Moreover, by alloying two TMDCs with different bandgaps, the resultant bandgap can be continuously tuned. For example, composite TMDC alloys $Mo_{1-x}W_xS_2$ [26, 27] and $MoS_{2(1-x)}Se_{2x}$ [28, 29] exhibit tunable direct bandgaps of 1.82–1.99 and 1.55–1.87 eV, respectively. More recently, an emerging 2D material, black phosphorus (BP), and its arsenic alloys (black $P_{(1-x)}As_x$), were also shown to exhibit a tunable bandgap, ranging from 0.15 to 0.3 eV [30]. These composite 2D materials are very promising for tunable optoelectronic applications in a broad range of wavelengths.

3 2D TMDC synthesis

The synthesis process and the quality of large-scale 2D TMDCs are critical for their device applications in nanophotonics and nanoelectronics. Recently, several techniques have been developed for the scalable synthesis of 2D materials. Different synthesis methods result in 2D TMDCs with diverse levels of quality in terms of the layer number control, the film size, the carrier mobility, the domain size, and the edges. These parameters can strongly affect the performance of 2D TMDC optoelectronic devices (such as photoresponsivity, response time, spectral response, and quantum efficiency). In this section, we will review the existing 2D TMDC synthesis methods, discuss the challenges, and highlight the potential applications

they may enable. In general, there are two strategies for synthesizing 2D TMDCs: (1) the top-down approach and (2) the bottom-up approach. Since much of the recent research on the synthesis of 2D materials was first conducted on MoS_2, we will use MoS_2 as a representative material of the TMDC family. Many of the methods mentioned below have also been demonstrated for other 2D TMDCs.

3.1 The top-down approach

Due to the weak van der Waals coupling between layers, single- or few-layer 2D material samples can be obtained by using micromechanical exfoliation. The early study of graphene heavily relied on such techniques [31], and many other 2D crystals [32–35] (such as MoS_2, WSe_2, and h-BN) can also be prepared in a similar way. Mechanical exfoliation can yield high-quality 2D crystal flakes, which is suitable for the investigation of their fundamental physical and chemical properties, or for the demonstration of novel device concepts in the laboratory setting. The exfoliated 2D crystals can be readily recognized when placed on suitable substrates that can yield a clear optical contrast between the sample flakes and the surrounding area (typically silicon with 90 or 290 nm of silicon oxide) [36–38]. The thickness of the SiO_2 layer is chosen to achieve the optimal contrast with a given 2D crystal, owing to the light interference (Fig. 2(a)). The number of the 2D atomic layers in a sample can be identified by the optical contrast with fairly good accuracy (Fig. 2(b)). The main advantage of this method is the ability to obtain 2D TMDCs that are single-crystalline, high-quality, and pristine. More recently, improved versions of the exfoliation technique have been developed by various research groups. To obtain TMDCs with controllable layer number, Castellanos-Gomez et al. [39] demonstrated the laser reduction of the thickness of exfoliated MoS_2 down to a single layer. Meanwhile, the exfoliated 2D crystals can also be transferred by mechanical techniques [40, 41] to the desired locations. Combining the exfoliation and transfer techniques (Fig. 2(c)), 2D material heterostructures containing stacks of 2D TMDCs (graphene, h-BN, and BP [42–44]) can be achieved, demonstrating a wide range of devices based on 2D material heterostructures [40, 45, 46].

Despite of the many benefits of the micromechanical exfoliation-based technique, this method cannot result in wafer-scale 2D materials for larger scale applications. An alternative top-down method for obtaining large-scale 2D TMDCs is based on the liquid phase exfoliation [47]. Such methods have been demonstrated to produce graphene samples with high yield [48]. Two-dimensional TMDC solutions (such as MoS_2 and WS_2) can also be obtained by sonication [49] or shearing [50] of a TMDC powder in appropriate solvents (e.g., N-methyl-pyrrolidone). A key factor in choosing the solvent is that the surface energy of the selected solvent needs to match that of the TMDC layer (Fig. 2(d)) for facilitating the layer separation. Furthermore, large-area 2D TMDC nanosheets can be obtained by vacuum filtration [49] (Fig. 2(e)) or spraying [51], which have also been developed based on the liquid phase approach. A major advantage of these production methods is that a large amount of the material can be obtained at a low cost. The main challenges, however, include the difficulty associated with accurately controlling the uniformity of the TMDC layer number and the yield of large-size flakes. Previously, a density gradient ultracentrifuge separation method [52] was used for controlling the graphene thickness. Thickness sorting of 2D TDMCs can also be realized by using a block copolymer dispersant [53]. The size and thickness were identified rapidly by using a normal benchtop centrifuge [54] (Fig. 2(f)). However, the resulting TMDCs were still mostly few-layer (ranging from 3 to 12 nm) rather than monolayer. To obtain monolayer TMDCs, chemical exfoliation-based approaches were also developed. By intercalating [47] lithium in the TMDC layers (Fig. 2(g)), the interlayer van der Waals bonding can be broken with external agitation, converting the bulk TMDC into monolayers. The main drawback of chemical exfoliation is that the lithium intercalation may lead to the 2H-to-1T phase transition in MoS_2, causing the semiconducting 2H MoS_2 to become the metallic 1T MoS_2. To alleviate this problem, Eda et al. [55] developed an additional annealing process at 300 °C, which could recover most of the MoS_2 2H phase. This method could facilitate the large-scale fabrication of monolayer MoS_2 (Fig. 2(h)); however, the crystal

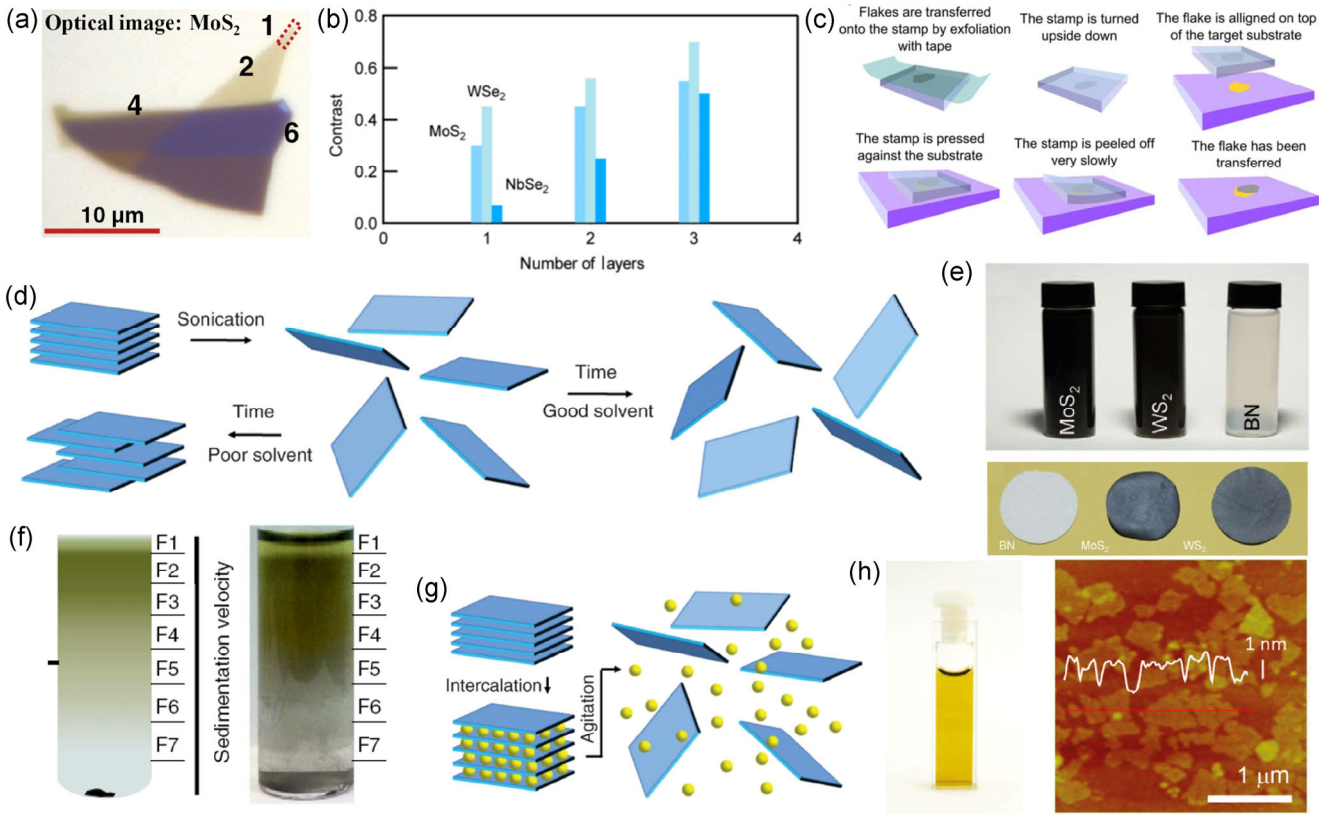

Figure 2 Top-down approach for TMDCs synthesis. (a) The optical image of the exfoliated monolayer MoS_2. Different thicknesses of MoS_2 identified by the optical contrast. (Reprinted with permission from Ref. [37], © WILEY-VCH Verlag GmbH & Co. KGaA 2012.) (b) The relation between the TMDC thickness and optical contact. (Reprinted with permission from Ref. [38], © IOP Publishing Ltd 2011.) (c) Fabrication of TMDC van der Waals heterostructures by using the dry transfer technique. (Reprinted with permission from Ref. [41], © IOP Publishing Ltd 2014.) (d) Schematic of the liquid exfoliation method. Choosing an appropriate solvent can make the layer exfoliation efficient. (Reprinted with permission from Ref. [47], © American Association for the Advancement of Science 2013.) (e) The solution of TMDCs and BN (top), and the films obtained by vacuum filtration (bottom). (Reprinted with permission from Ref. [49], © American Association for the Advancement of Science 2011.) (f) Different sizes of MoS_2 selected by centrifugation and fractionation. (Reprinted with permission from Ref. [54], © Nature Publishing Group 2014.) (g) Ions intercalation in the TMDC layers for breaking the bulk into monolayers. (Reprinted with permission from Ref. [47], © American Association for the Advancement of Science 2013.) (h) Chemically exfoliated MoS_2 suspension in water (left) and AFM image (right), confirming the monolayer thickness and large-scale production. (Reprinted with permission from Ref. [55], © American Chemical Society 2012.)

size of individual flakes is still limited to ~1 μm.

Among all the top-down approaches reported in the literature, the mechanical and chemical exfoliation techniques can provide advantages during the early stages of material and device search for a novel 2D material. Mechanical exfoliation can yield high-quality 2D crystals for fundamental physics and laboratory demonstration of novel device concepts, albeit small in size. Chemical exfoliation can be used for large-scale fabrication of 2D crystals with high yield and low cost for some specific applications.

3.2 The bottom-up approach

Chemical vapor deposition (CVD) based methods are widely adopted for fabricating large-area 2D TMDCs. The bottom-up CVD methods have many advantages compared with the top-down approach methods. The growth instruments are inexpensive and versatile, and the resulting material quality is relatively high. Furthermore, compared with the top-down approach methods, the size of the continuous material film can be much larger.

3.2.1 *Synthesis of 2D TMDC materials*

One of the most popular CVD methods [56, 57] for growing MoS_2 uses S and MoO_3 as precursors (Fig. 3(a)). The growth of MoS_2 can be further promoted by pretreating the substrate by using organic molecules as a seed layer (such as perylene-3,4,9,10-tetracarboxylic acid tetrapotassium salt (PTAS)). Using this method, MoS_2 can be grown on a diverse range of insulating substrates [58] such as SiO_2, sapphire, and quartz. Hence, the film transfer step that is needed for CVD-grown graphene is skipped by using this method, and the drawbacks associated with this step, such as etchant contamination, possible physical film damage and wrinkle formation are avoided. Moreover, two-inch wafer-scale few-layer MoS_2 can also be grown by using S and MoO_3 as precursors in a two-step thermal process [59]. Utilizing this method, prototypes of MoS_2 integrated devices and circuits [60, 61] have been demonstrated. On the other hand, Liu et al. [62] demonstrated that a $(NH_4)_2MoS_4$ solution annealed with S can also result in few-layer MoS_2 on insulating substrates (Fig. 3(b)). The typical crystal size of CVD-grown MoS_2 ranges from tens of μm to over 100 μm. van der Zande et al. optimized the growth condition and demonstrated, by using a similar method, triangular single-crystal MoS_2 with lateral size up to 120 μm [63]. Furthermore, tilt and mirror twin boundaries were also formed by lines of 8- and 4-member rings. Najmaei et al. [64] reported the observation of the MoS_2 grain boundaries consisting of 5- and 7-member rings. However, wafer-scale synthesis of single-layer MoS_2 remains a significant challenge. The poly-crystallinity of the resulting samples, the lack of understanding of the defects formation and control during growth, and the difficulties associated with achieving consistent and reproducible growth results are the main challenges associated with these synthesis approaches. More recently, Kang et al. [65] successfully synthesized 4-inch wafer-scale films of monolayer MoS_2 and WS_2 with excellent coverage (Fig. 3(c)) by using a method based on the metal–organic chemical vapor deposition (MOCVD). $Mo(CO)_6$, $W(CO)_6$, $(C_2H_5)_2S$, and H_2 were used as gas-phase precursors, and argon served as the carrier gas. The yield of field effect transistors (FETs) reached 99%, and the mobility of MoS_2 was as high as 30 cm^2/Vs, which was comparable to the exfoliated MoS_2. It typically takes 26 h to form a uniform coverage [66]. These results revealed a promising potential for the wafer-scale production of 2D TMDC-based electronics and photonics.

3.2.2 *Synthesis of 2D TMDC heterostructures*

Most recently, researchers have also made significant progress in developing 2D TMDC heterojunctions by using CVD-based methods. There are two main types of TMDC heterojunctions: (1) the in-plane heterojunctions that laterally connect one type of TMDC material with another TMDC material, and (2) the vertical heterojunctions that stack one layer of TMDC materials atop another layer of TMDC. Here, we will mainly focus on the growth of lateral heterojunctions because such junctions can only be obtained through direct synthesis, but generally not by exfoliation and transfer-based techniques.

By mixing similar amounts of WSe_2 and $MoSe_2$ powders as precursors, lateral $MoSe_2$–WSe_2 heterostructures can be directly grown by using the vapor–solid method. The resulting material has been shown to possess enhanced PL [67, 68]. Gong et al. [69] reported a one-step growth process for synthesizing both the in-plane and vertical heterostructures by controlling the vapor phase growth temperature. The abrupt lateral interface of in-plane heterojunctions between WS_2 and MoS_2 monolayers was observed by employing high-resolution transmission electron microscopy (TEM). Chen et al. [70] synthesized lateral WS_2/MoS_2 heterojunctions by using ammonium molybdate tetrahydrate and ammonium tungstate hydrate as the sources for Mo and W elements in an atmospheric CVD (APCVD) process. Furthermore, Duan et al. [71], Li et al. [72], Gong et al. [73], and Chen et al. [74] demonstrated two-step processes for growing in-plane heterostructures with improved controllability over the sequence order of 2D TMDCs in the heterostructures and for preventing the formation of alloys. In these techniques, the first type of TMDC was typically grown by using a CVD process. The precursors were then switched to allow the epitaxial synthesis of the second layer of a different TMDC material. The as-grown 2D heterojunctions typically

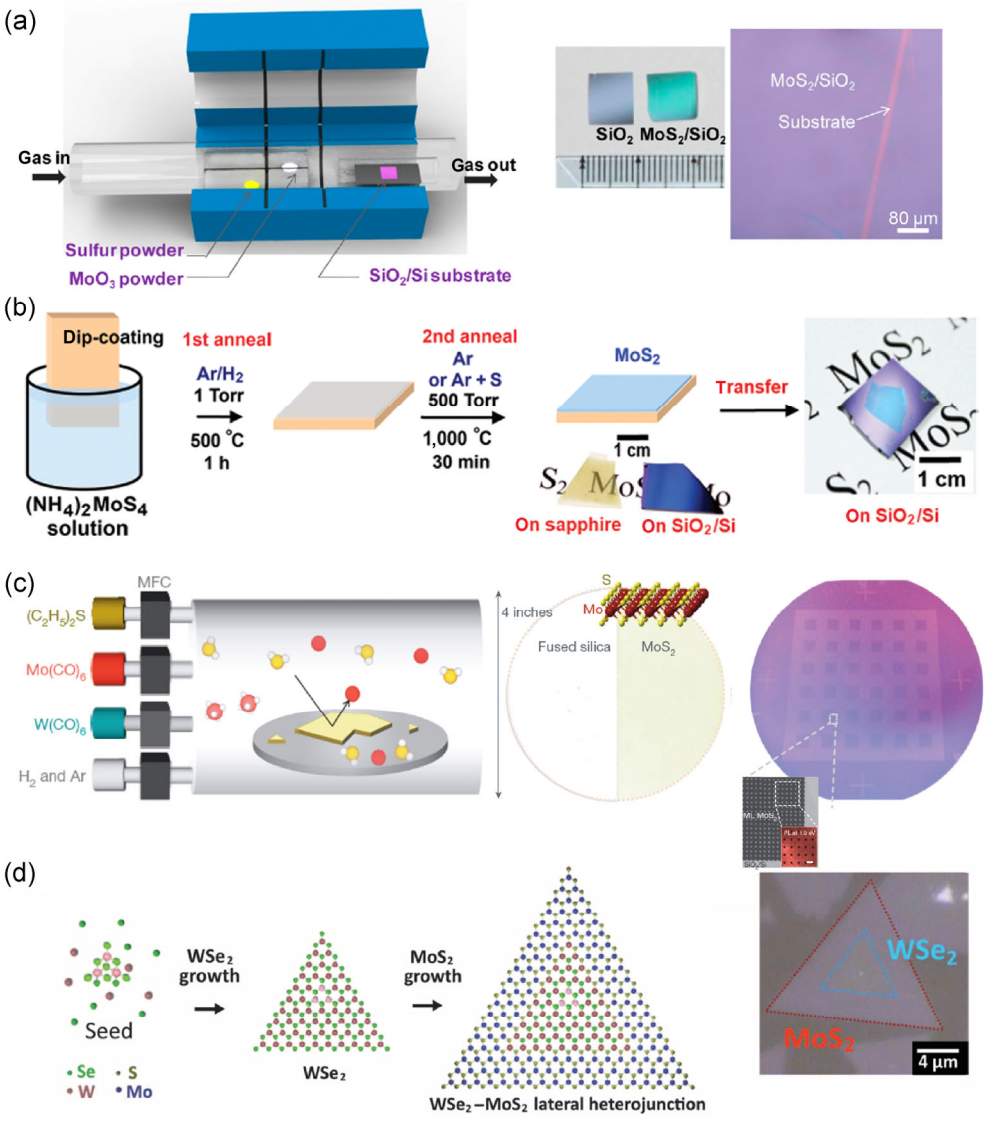

Figure 3 Bottom-up approach for TMDCs synthesis. (a) Schematic of the CVD growth method for MoS_2 by using S and MoO_3 powders as precursors (left), and the large-area MoS_2 after growth. (Reprinted with permission from Ref. [57], © American Chemical Society 2014.) (b) CVD growth of MoS_2 by a dip-coating precursor, followed by annealing in Ar and S vapor. (Reprinted with permission from Ref. [62], © American Chemical Society 2012.) (c) The 4-inch wafer-scale growth of monolayer MoS_2 by MOCVD. (Reprinted with permission from Ref. [65], © Nature Publishing Group 2015.) (d) Schematic of the CVD synthesis process for growing WSe_2–MoS_2 in-plane heterostructures, and an optical image of the resulting material. (Reprinted with permission from Ref. [72], © American Association for the Advancement of Science 2015.)

have a triangular-shaped region of one type of 2D TMDC surrounded by another TMDC material. Zhang et al. [75] demonstrated the use of WO_{3-x}/MoO_{3-x} core shell structure as a precursor for the controllable growth of MoS_2/WS_2 heterostructures. Since the sublimation temperature of WO_{3-x} (core) is naturally higher than that of MoO_{3-x} (shell), the sequence of MoS_2 and WS_2 can be controlled by controlling the furnace temperature at different stages of the synthesis process.

Growth by CVD can be used for realizing large-scale and high-quality films suitable for optoelectronics applications both at the research- and industry-level. Currently, a minor drawback of CVD-synthesized TMDC films is that the as-grown TMDCs are mostly polycrystalline with grain boundaries, which can slightly degrade the electrical and optical properties of

the resulting materials, compared with single-crystalline samples. An additional direction for improving CVD-synthesized TMDCs is the growth of large-area single-crystal films, which can enable real optoelectronics applications.

4 Photonics of TMDCs

4.1 2D TMDC-based photodetectors

The diverse optical properties of 2D TMDCs, with their bandgaps ranging from the IR to the near UV energy range, the direct and indirect transitions that depend on the number of layers, and their large excitonic binding energies are the unique features that have propelled intensive effort toward developing novel optical devices based on these materials. Two-dimensional TMDC photodetectors exhibit decent responsivity from the IR to the near UV range. The first reported monolayer MoS_2 photodetector [76] has exhibited the responsivity of 7.5 mA/W in the visible range. Choi et al. [77] demonstrated the responsivity of ~100 mA/W by using a multi-layer MoS_2, which is much higher than that reported for a typical graphene photodetector (typically 0.2 mA/W [9]) in the visible range. This higher responsivity can be explained by the stronger light–matter interaction and photon absorption in TMDC materials. Moreover, Lee et al. [19] utilized the dependence of the optical bandgap on the layer number in atomically thin MoS_2, and revealed that single- and bilayer MoS_2 are suitable for the detection of green light, while trilayer MoS_2 are suitable for the detection of red light. However, the response speed is relatively slow (ranging from microseconds to seconds) owing to the trapping of photocarriers. TMDC photodetectors can hence be used as imaging sensor arrays that are typically less demanding with respect to the operating speed but require higher responsivity.

Several high-gain TMDC-based photodetector devices have also been demonstrated. Lopez-Sanchez et al. [78] have fabricated monolayer MoS_2 phototransistors with ultra-high responsivity, up to 880 A/W for the wavelength of 561 nm, and with the operational wavelength in the 400–680 nm range. Such high responsivity corresponds to external quantum efficiencies well above 100%, indicating the existence of an internal gain mechanism. The photocurrent gain can be viewed as one incident photon generating multiple charge carriers and the electrical charges recirculating many times owing to the long trapped-charge lifetime in MoS_2. Furchi et al. [79] revealed that the photoconductive gain in MoS_2 stems from the trapping of either the electrons or holes, which yields prolonged photocarrier lifetime and in turn high photoconductive gain. The band tail trap states and mid-gap states in MoS_2 were typically induced by structural defects or disorder. These trapped states in MoS_2 enhance the photocurrent response and hence the responsivity of the detectors. A similar work [80] on a multi-layer WS_2 phototransistor demonstrated responsivities on the order of 5.7 A/W and an external quantum efficiency (EQE) of 1,118% at the wavelength of 633 nm. Moreover, Mo-doped $ReSe_2$ nanosheets [81] were shown to exhibit the photoresponsivity of 55.5 A/W and the EQE of 10,893% at the wavelength of 633 nm in an ammonia environment. Another strategy to further improve the efficiency and photoresponsivity for this class of devices is to create heterojunctions of TMDC materials and other 2D materials such as MoS_2/graphene [82, 83], WS_2/graphene [45], and MoS_2/carbon nanotubes (CNTs) [84]. The built-in electric field in the TMDC heterojunction can allow for the more efficient separation of the electron–hole pairs. The responsivity enhancement strategies discussed above, however, generally come at the cost of decreased operating speed. Since these devices rely on band tail states or mid-gap states for realizing high photocurrent gains, this mechanism is fundamentally slow and the response time is typically on the order of milliseconds to seconds.

Another common approach for enhancing photonic absorption in materials utilizes optical resonances. Lin et al. [85] demonstrated plasmonic enhancement of photocurrent in MoS_2 field-effect-transistor decorated with gold nanoparticles. By tuning the plasmonic resonance of silica–gold nanoshells to the energy range of the excitonic transitions, Sobhani et al. [86] further demonstrated significant enhancement of the optical absorption in MoS_2 crystals, yielding a three-fold improvement of the photocurrent response. Moreover, the hot electrons induced by the strong

local field in 2D materials can also result in structural phase transformations from the semiconducting 2H phase to the metallic 1T phase. Kang et al. [87] demonstrated, by studying the vibrational properties and PL in MoS_2, that the plasmon-induced hot electrons were responsible for such transition. Using plasmonic cavities with resonant energies matching the bandgap of TMDCs, one can even further enhance the absorption properties of these materials. Akselrod et al. [88] showed that using this concept and colloidally synthesized nano-cavities, one can enhance the PL intensities of 2D semiconductors by 2,000-fold. This study suggested that one may engineer the plasmonic resonators to better manipulate the light–matter interaction in 2D materials. By using a similar approach, Lee et al. [89] showed how the geometry, the parameters of bowtie nanoarrays, and the exciton–plasmon coupling can modify the emission and excitation processes. These effects can lead to the ability to tune the spectrum and the intensity of the PL. Strong exciton–plasmon coupling, achieved at low temperatures, can result in Fano-type line shapes in the reflection spectrum. Najmaei et al. [90] further explored the possible plasmonic-2D material hybrids by designing antennas with tunable resonances. Heating can be observed as changes in the PL spectrum, which directly results from an increased absorption in the 2D material layer and the non-radiative means of relaxation.

4.2 2D TMDC-based LEDs

Since the early 1960s, the commercialization of the LED technology has led to technological revolutions in the areas of solid-state lighting, displays, sensors, and data transmission. Recent developments in the study of 2D TMDCs have also provided a glimpse of the possibilities for building atomically thin LEDs. The fact that many of these TMDCs possess a direct bandgap when thinned down to a single atomic layer motivates potential applications for optical emission. A number of research groups [91–95] have demonstrated electroluminescence (EL) in a variety of 2D TMDCs, including MoS_2, WS_2, and WSe_2, along with various heterostructures comprised of a combination of these materials.

Early demonstrations of EL in monolayer MoS_2 by Sundaram et al. [91] made use of the Schottky barrier between the MoS_2 and the Cr/Au metal contact, with the EL being attributed to hot carrier processes localized in the proximity of the contacts. Light emission, demonstrated in other TMDCs, has soon followed, with Jo et al. [21] reporting EL in monolayer and bilayer WS_2 by using an ionic liquid-gated FET structure to form a p–n junction in the WS_2 channel. Electrons and holes are simultaneously injected from the contacts and recombine at the junction to emit light. Furthermore, multiple reports of p–n junctions using lateral WSe_2 channels have demonstrated EL based on the radiative recombination of the injected carriers. In all cases, electrostatic gating was used to create the adjacent n-doped and p-doped regions in the WSe_2 channel [92–94]. The EL efficiency, defined as the ratio between the number of photons generated and the number of electron–hole pairs injected, has been reported to range from 0.1% to 1%, with driving currents ranging from 35 up to 200 nA. The peak emission wavelength range extends from ~752 up to ~800 nm, depending on the device design and the operating temperature [92–94]. Compared with the EL demonstrated by Sundaram et al. in a MoS_2–metal Schottky junction, the EL based on the WSe_2 p–n junction exhibited a significant increase in the emission efficiency. Interestingly, the driving current magnitude was orders of magnitude lower. Figure 4(a) provides an illustration of a WSe_2 p–n junction presented by Ross et al. [93]. It has been clarified that the EL produced in these WSe_2-based p–n junctions stems from excitons that equally propagate in the valleys located at the K and K′ points in the Brillouin zone of WSe_2. Using this unique feature, Zhang et al. [95] successfully employed the valley degrees of freedom of a few-layer WSe_2 to generate circularly polarized EL based on a p–i–n junction device.

Light emission has also been demonstrated in vertical heterostructures based on 2D TMDCs [96–98]. A vertical p–n junction using n-type MoS_2 and p-type silicon was demonstrated by Lopez-Sanchez et al. [96], with the wavelength of 694 nm at the peak intensity, as shown in Fig. 4(b). The light emission was achieved with a significantly lower power density compared with the value of 15 kW/cm^2 reported for previous devices that used hot carrier injection as

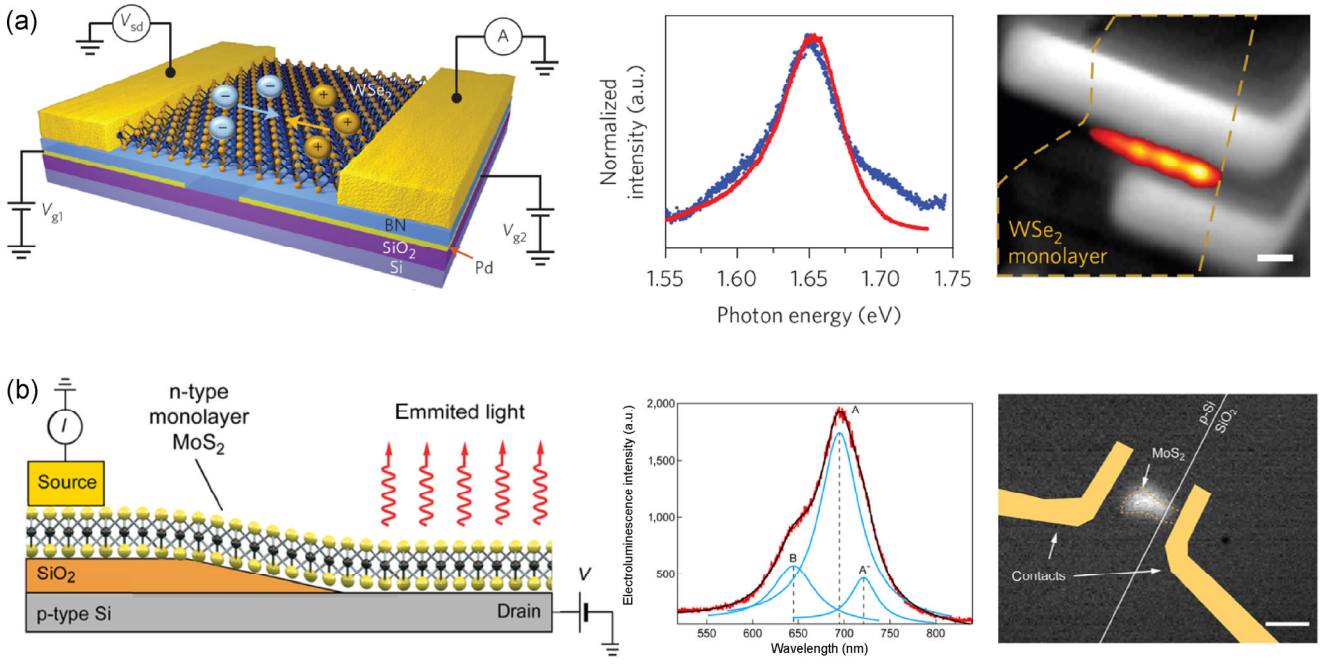

Figure 4 Two-dimensional TMDC LEDs. (a) Schematic of a TMDC-based LED device, the EL spectrum at 300 K generated with a 5 nA current (shown in blue) along with the corresponding PL spectrum (shown in red), and an EL image with superimposed greyscale device image are shown for a p–n junction structure based on electrostatically gated WSe_2. (Reprinted with permission from Ref. [93], © Nature Publishing Group 2014.) (b) Schematic of the EL spectrum at room temperature generated with a 1.8 μA current (with A exciton, B exciton, A^- trion contributions detailed), and an EL image with superimposed device drawing are shown for a vertical p-type Si/n-type MoS_2 p–n junction heterostructure. (Reprinted with permission from Ref. [96], © American Chemical Society 2014.)

the emission mechanism [91]. EL from vertical p–n junction heterostructures consisting of a monolayer n-type MoS_2 and p-type WSe_2 has been demonstrated with exciton energy peaking around 792 nm in the EL spectra [97]. Finally, more complex vertical heterostructures with carefully designed graphene/BN/TMDC/BN/graphene quantum well structures have been shown to emit light with EL efficiencies reaching ~1%. It has been shown that with multiple monolayer TMDCs stacked together (but separated by insulating h-BN layers), it is possible to achieve up to 8.4% EL efficiency [98].

Owing to the direct bandgap nature of many monolayer TMDCs, the 2D TMDCs-based LEDs already exhibit relatively efficient light emission. Moreover, the wavelength of the emitted light can be tuned over a wide spectral range by selecting and combining 2D TMDCs, as well as other 2D materials, in suitable heterostructures. As the 2D material synthesis and 2D device fabrication techniques continue to improve, higher quality TMDCs with better interface are expected to further enhance the light emission efficiency, which is very promising for a broad range of optoelectronic applications. As a final note, owing to the direct bandgap of many monolayer TMDCs, TMDC-based nanolasers may also be realized through their integration with nanocavities. Wu et al. [99] demonstrated an ultra-low threshold WSe_2 nanolaser operating in the visible spectrum. Yu et al. [100] demonstrated another type of nanolaser by using a monolayer of WS_2 sandwiched between an HSQ layer and a Si_3N_4 layer to form a microdisk resonator. Salehzadeh et al. [101] also demonstrated a similar microdisk structure by using MoS_2. Moreover, electrostatic gating of TMDCs may allow an additional control over the emission characteristics of such nanolasers, although no such devices have been experimentally reported at present. Although there have been a few recent demonstrations (as discussed above), the exploration of TMDCs for laser applications is still in its infancy. The prospects of the scalable fabrication of such devices, compatibility with integrated

photonics, and the possibility of electrically pumped operation remain to be fully investigated.

5 Outlook

5.1 Challenges

Three major challenges are associated with the development of 2D TMDC photonic devices: (1) the growth of high-quality TMDC materials over a large area, (2) the realization of clean interfaces between TMDCs and other materials, and (3) the formation of low-resistance contacts with TMDCs. Although we have seen substantial improvement in the area of 2D TMDC synthesis, existing CVD TMDCs are still limited in terms of their grain size (typically 10–100 μm) and overall material quality. Synthesizing large-area, single-crystalline TMDCs with controllable thickness and with low defects density remains highly challenging. The defects can act as non-radiative recombination centers that degrade the photocurrent, as well as the light emission efficiency and operating speed of the optoelectronic devices. Moreover, creating sharp and clean interfaces between TMDCs with other materials remains an issue. Identifying suitable materials and innovative solutions for forming low-resistance Ohmic contacts with TMDCs is also a glaring need. In the long run, issues related to the material uniformity over a large area, the yield of the device fabrication, and the reliability of the device operation will require significant effort to be resolved before the technology may be utilized on a wider scale. Meanwhile, notwithstanding many remaining challenges, the future 2D optoelectronics research offers many opportunities; these are discussed below.

5.2 Opportunities

Since 2004, the research on graphene has been promising many possibilities for its use in electronic and optoelectronic applications. Following the rediscovery of MoS_2 in 2011 [33, 102–104], TMDCs have been found to be promising 2D semiconductors for optoelectronic applications, owing to their wide range of available bandgaps (TiS_2 and $TiSe_2$ with bandgaps of ~0.3 eV [105–107] to HfS_2 with the bandgap of >2.0 eV [108, 109]). In recent years, van der Waals heterostructures [42] that combine TMDCs with, e.g., graphene and h-BN, have attracted significant attention. By carefully choosing the stack sequence, numerous novel vertical heterostructure devices based on 2D materials have been demonstrated, including the Schottky junctions [44, 82], p–n junctions [84, 97], and tunneling structures [40, 110]. The optoelectronic devices based on heterostructures exhibit outstanding performance. For example, photodetectors based on graphene/TMDC/graphene [45, 82] (Fig. 5(a)) exhibit an external quantum efficiency of up to 55%. Most recently, LEDs based on graphene/h-BN/TMDC/h-BN/graphene quantum well structures [98] show external quantum efficiencies of nearly 10% (Fig. 5(b)). Moreover, gating of the graphene–TMDC junctions can be used for tuning the Fermi level of the heterostructure, resulting in tunable optoelectronic devices. Lee et al. [46] and Furchi et al. [111] demonstrated gate-tunable p–n heterojunctions using a van der Waals assembly of monolayer MoS_2/WSe_2 (Fig. 5(c)). However, the detection spectral ranges of most TMDC photodetectors to date are limited to the visible range.

The extension of the detection range to near and mid-IR range can be realized by hybridizing TMDCs with BP, which has the bandgap of ~0.3 eV that can bridge the zero bandgap of graphene and some commonly used TMDCs such as MoS_2 and WSe_2, which have bandgaps in the 1.5–2.5 eV range. Buscema et al. [112] demonstrated the power generation from a BP p–n junction at 940 nm (Fig. 6(a)). Moreover, BP has the unique property of possessing in-plane anisotropy, which could lead to new optical device concepts. Researchers at Yale/USC [113–115] used IR spectroscopy for identifying the crystal orientation. It was observed that the BP's extinction spectrum reaches its maximal values for incident light polarized along the armchair direction, owing to the anisotropic absorption (Fig. 6(b)). Most recently, it has been shown that a monolayer BP [116] exhibits a PL spectrum with strong anisotropy (Fig. 6(c)). Yuan et al. [117] demonstrated a broadband multi-layer BP (30–50 nm) photodetector, with polarization sensitivity over wavelengths in the 400–1,700 nm range (Fig. 6(d)). Meanwhile, the investigation of TMDC lasers is also in its infancy, with relatively low quantum efficiencies (0.3%) obtained up to date [100], and more studies are required for

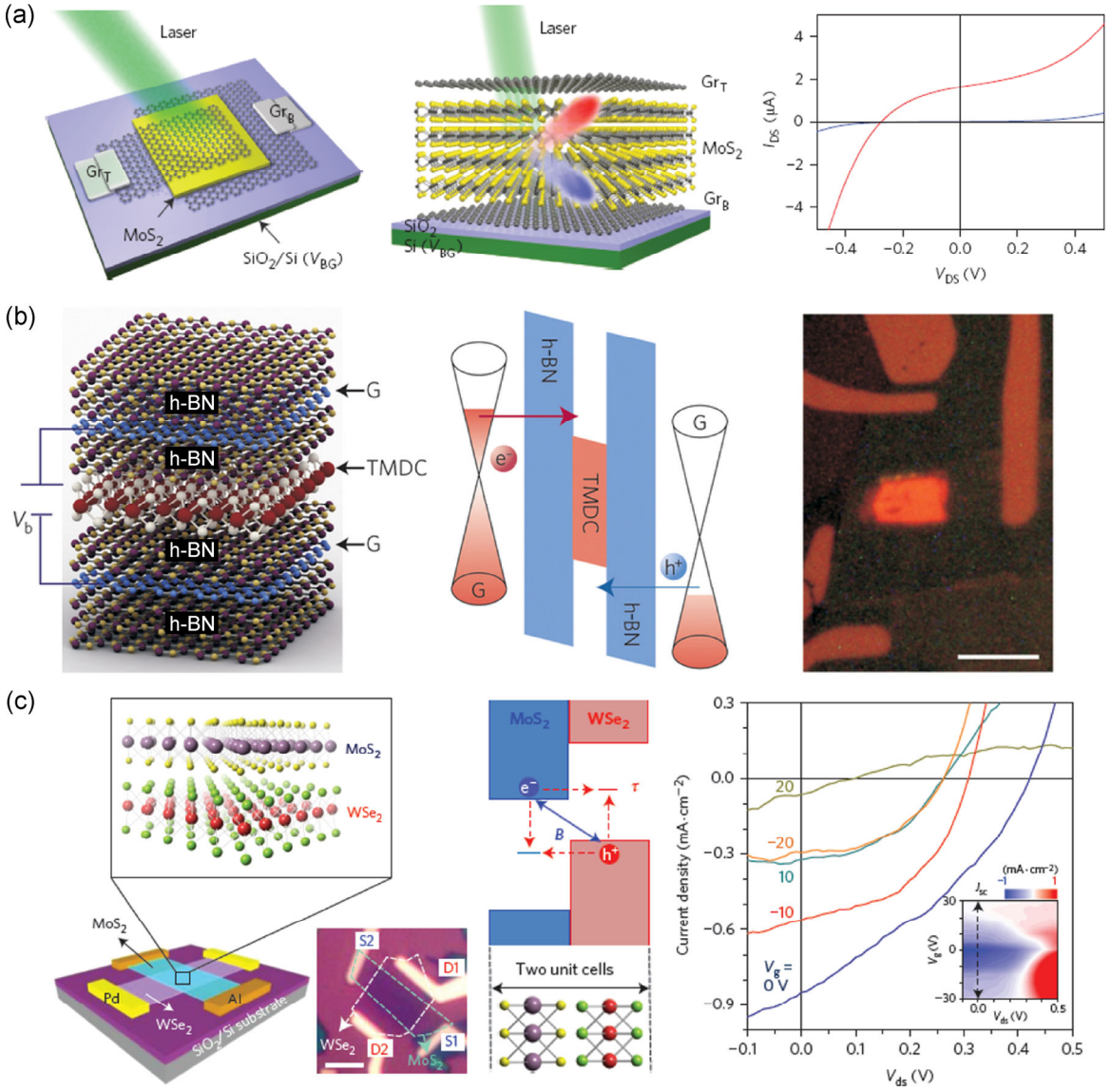

Figure 5 Photonics of TMDC heterojunctions. (a) Schematic of a graphene–MoS_2–graphene heterojunction photodetector showing a maximal external quantum efficiency of 55%. (Reprinted with permission from Ref. [82], © Nature Publishing Group 2013.) (b) Schematic of a graphene/BN/TMDC/BN/graphene LED with external quantum efficiency of ~10%. (Reprinted with permission from Ref. [122], © Nature Publishing Group 2015.) (c) Schematic of a MoS_2/WSe_2 photovoltaic device with gate-tunable *I*–*V* performance. (Reprinted with permission from Ref. [46], © Nature Publishing Group 2015.)

better understanding the governing mechanisms. Enhancing the quantum efficiency of nanolasers may also be achieved by utilizing 2D heterostructures. Moreover, owing to the broken inversion symmetry in TMDCs, the valley degree of freedom in TMDCs provides ample opportunities for realizing valleytronic devices. Valley Hall and spin Hall effects [118] were predicted to coexist in TMDC systems. Experimental results [25, 103, 119] have shown the valley polarization in monolayer MoS_2 controlled by circularly polarized light. Jones et al. [120] demonstrated that valley coherence can be generated and detected, which is an important step towards coherent valleytronics. Yuan et al. [121] demonstrated that a spin-coupled valley photocurrent can be modulated by an electric field. The physics of valleys in the *k*-space mimic that of spin, which has the potential to realize valley-based low-power optoelectronics.

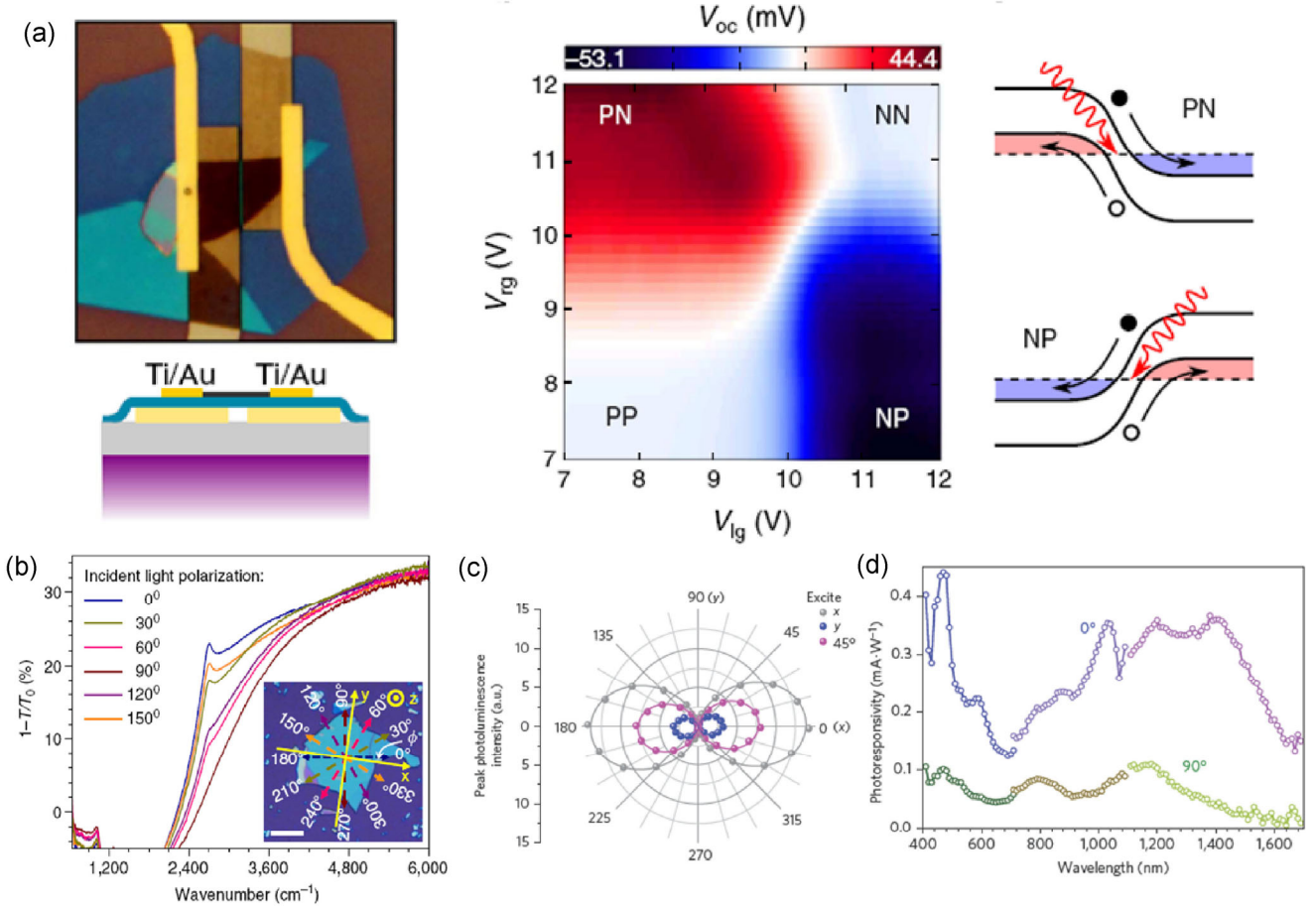

Figure 6 Photonics of BP. (a) The BP p–n junction device tuning by the dual-gate, output voltage under different gate voltages and its band diagram. (Reprinted with permission from Ref. [112], © Nature Publishing Group 2014.) (b) The polarization-resolved IR relative extinction spectra of a few-layer BP. (Reprinted with permission from Ref. [113], © Nature Publishing Group 2014.) (c) The monolayer BP, exhibiting a strongly anisotropic PL spectrum. (Reprinted with permission from Ref. [116], © Nature Publishing Group 2015.) (d) The multi-layer BP, exhibiting broadband anisotropic absorption in the 400–1,700 nm range. (Reprinted with permission from Ref. [117], © Nature Publishing Group 2015.)

6 Conclusions

In this review, we have summarized the recent progress in TMDC-based optoelectronic devices. The TMDC-based photodetectors, LEDs, and lasers with significant performance were discussed here. Benefiting from the direct bandgap in many TMDC monolayers, the 2D TMDCs optoelectronic devices exhibit higher efficiency than their bulk forms. Combining TMDCs with other 2D materials (such as graphene, h-BN, and BP), the bandgap can cover a wide spectral range, from visible to mid-IR. The fabrication of TDMCs can utilize both top-down and bottom-up approaches. The grain-size, interface, and metal contacts of TMDC materials demand further investigation. The wide variety of available 2D TMDC materials, together with other 2D materials (such as graphene and BP) are very promising for realizing novel devices for light detection, emission, modulation, and manipulation, with many applications in communication, sensing, computation, and healthcare.

Acknowledgements

The authors acknowledge support from the National Science Foundation (No. EFMA-1542815), Army Research Laboratory, and USC Zumberge Individual Award.

References

[1] Geim, A. K.; Novoselov, K. S. The rise of graphene. *Nat. Mater.* **2007**, *6*, 183–191.

[2] Geim, A. K. Graphene: Status and prospects. *Science* **2009**, *324*, 1530–1534.

[3] Novoselov, K. S.; Fal'ko, V. I.; Colombo, L.; Gellert, P. R.; Schwab, M. G.; Kim, K. A roadmap for graphene. *Nature* **2012**, *490*, 192–200.

[4] Zhang, Y. B.; Tan, Y.-W.; Stormer, H. L.; Kim, P. Experimental observation of the quantum Hall effect and Berry's phase in graphene. *Nature* **2005**, *438*, 201–204.

[5] de Abajo, F. J. G. Graphene nanophotonics. *Science* **2013**, *339*, 917–918.

[6] Freitag, M. Graphene: Nanoelectronics goes flat out. *Nat. Nanotechnol.* **2008**, *3*, 455–457.

[7] Meric, I.; Han, M. Y.; Young, A. F.; Ozyilmaz, B.; Kim, P.; Shepard, K. L. Current saturation in zero-bandgap, top-gated graphene field-effect transistors. *Nat. Nanotechnol.* **2008**, *3*, 654–659.

[8] Yan, J.; Zhang, Y. B.; Kim, P.; Pinczuk, A. Electric field effect tuning of electron–phonon coupling in graphene. *Phys. Rev. Lett.* **2007**, *98*, 166802.

[9] Freitag, M.; Low, T.; Xia, F. N.; Avouris, P. Photoconductivity of biased graphene. *Nat. Photon.* **2013**, *7*, 53–59.

[10] Ju, L.; Geng, B. S.; Horng, J.; Girit, C.; Martin, M.; Hao, Z.; Bechtel, H. A.; Liang, X. G.; Zettl, A.; Shen, Y. R. et al. Graphene plasmonics for tunable terahertz metamaterials. *Nat. Nanotechnol.* **2011**, *6*, 630–634.

[11] Grigorenko, A. N.; Polini, M.; Novoselov, K. S. Graphene plasmonics. *Nat. Photon.* **2012**, *6*, 749–758.

[12] Mueller, T.; Xia, F. N.; Avouris, P. Graphene photodetectors for high-speed optical communications. *Nat. Photon.* **2010**, *4*, 297–301.

[13] Liu, M.; Yin, X. B.; Ulin-Avila, E.; Geng, B. S.; Zentgraf, T.; Ju, L.; Wang, F.; Zhang, X. A graphene-based broadband optical modulator. *Nature* **2011**, *474*, 64–67.

[14] Mueller, T.; Xia, F. N.; Freitag, M.; Tsang, J.; Avouris, P. Role of contacts in graphene transistors: A scanning photocurrent study. *Phys. Rev. B* **2009**, *79*, 245430.

[15] Wang, Q. H.; Kalantar-Zadeh, K.; Kis, A.; Coleman, J. N.; Strano, M. S. Electronics and optoelectronics of two-dimensional transition metal dichalcogenides. *Nat. Nanotechnol.* **2012**, *7*, 699–712.

[16] Peng, B.; Ang, P. K.; Loh, K. P. Two-dimensional dichalcogenides for light-harvesting applications. *Nano Today* **2015**, *10*, 128–137.

[17] Liu, E. F.; Fu, Y. J.; Wang, Y. J.; Feng, Y. Q.; Liu, H. M.; Wan, X. G.; Zhou, W.; Wang, B. G.; Shao, L. B.; Ho, C.-H. et al. Integrated digital inverters based on two-dimensional anisotropic ReS_2 field-effect transistors. *Nat. Commun.* **2015**, *6*, 6991.

[18] Zhao, H.; Guo, Q. S.; Xia, F. N.; Wang, H. Two-dimensional materials for nanophotonics application. *Nanophotonics* **2015**, *4*, DOI: 10.1515/nanoph-2014-0022.

[19] Lee, H. S.; Min, S.-W.; Chang, Y.-G.; Park, M. K.; Nam, T.; Kim, H.; Kim, J. H.; Ryu, S.; Im, S. MoS_2 nanosheet phototransistors with thickness-modulated optical energy gap. *Nano Lett.* **2012**, *12*, 3695–3700.

[20] Tonndorf, P.; Schmidt, R.; Böttger, P.; Zhang, X.; Börner, J.; Liebig, A.; Albrecht, M.; Kloc, C.; Gordan, O.; Zahn, D. R. et al. Photoluminescence emission and Raman response of monolayer MoS_2, $MoSe_2$, and WSe_2. *Opt. Express* **2013**, *21*, 4908–4916.

[21] Jo, S.; Ubrig, N.; Berger, H.; Kuzmenko, A. B.; Morpurgo, A. F. Mono- and bilayer WS_2 light-emitting transistors. *Nano Lett.* **2014**, *14*, 2019–2025.

[22] Zhao, H.; Wu, J. B.; Zhong, H. X.; Guo, Q. S.; Wang, X. M.; Xia, F. N.; Yang, L.; Tan, P.-H.; Wang, H. Interlayer interactions in anisotropic atomically thin rhenium diselenide. *Nano Res.* **2015**, *8*, 3651–3661.

[23] Duerloo, K.-A. N.; Li, Y.; Reed, E. J. Structural phase transitions in two-dimensional Mo- and W-dichalcogenide monolayers. *Nat. Commun.* **2014**, *5*, 4214.

[24] Li, Y.; Duerloo, K.-A. N.; Wauson, K.; Reed, E. J. Structural semiconductor-to-semimetal phase transition in two-dimensional materials induced by electrostatic gating. *Nat. Commun.* **2016**, *7*, 10671.

[25] Cao, T.; Wang, G.; Han, W. P.; Ye, H. Q.; Zhu, C. R.; Shi, J. R.; Niu, Q.; Tan, P. S.; Wang, E. G.; Liu, B. L. et al. Valley-selective circular dichroism of monolayer molybdenum disulphide. *Nat. Commun.* **2012**, *3*, 887.

[26] Chen, Y. F.; Xi, J. Y.; Dumcenco, D. O.; Liu, Z.; Suenaga, K.; Wang, D.; Shuai, Z. G.; Huang, Y.-S.; Xie, L. M. Tunable band gap photoluminescence from atomically thin transition-metal dichalcogenide alloys. *ACS Nano* **2013**, *7*, 4610–4616.

[27] Chen, Y. F.; Dumcenco, D. O.; Zhu, Y. M.; Zhang, X.; Mao, N. N.; Feng, Q. L.; Zhang, M.; Zhang, J.; Tan, P.-H.; Huang, Y.-S. et al. Composition-dependent Raman modes of $Mo_{1-x}W_xS_2$ monolayer alloys. *Nanoscale* **2014**, *6*, 2833–2839.

[28] Gong, Y. J.; Liu, Z.; Lupini, A. R.; Shi, G.; Lin, J. H.; Najmaei, S.; Lin, Z.; Elías, A. L.; Berkdemir, A.; You, G. et al. Band gap engineering and layer-by-layer mapping of selenium-doped molybdenum disulfide. *Nano Lett.* **2014**, *14*, 442–449.

[29] Mann, J.; Ma, Q.; Odenthal, P. M.; Isarraraz, M.; Le, D.; Preciado, E.; Barroso, D.; Yamaguchi, K.; von Son Palacio, G.; Nguyen, A. et al. 2-dimensional transition metal dichalcogenides with tunable direct band gaps: $MoS_{2(1-x)}$ Se_{2x}

monolayers. *Adv. Mater.* **2014**, *26*, 1399–1404.

[30] Liu, B. L.; Köpf, M.; Abbas, A. A.; Wang, X. M.; Guo, Q. S.; Jia, Y. C.; Xia, F. N.; Weihrich, R.; Bachhuber, F.; Pielnhofer, F. et al. Black arsenic-phosphorus: Layered anisotropic infrared semiconductors with highly tunable compositions and properties. *Adv. Mater.* **2015**, *27*, 4423–4429.

[31] Novoselov, K. S.; Geim, A. K.; Morozov, S. V.; Jiang, D.; Zhang, Y.; Dubonos, S. V.; Grigorieva, I. V.; Firsov, A. A. Electric field effect in atomically thin carbon films. *Science* **2004**, *306*, 666–669.

[32] Novoselov, K. S.; Jiang, D.; Schedin, F.; Booth, T. J.; Khotkevich, V. V.; Morozov, S. V.; Geim, A. K. Two-dimensional atomic crystals. *Proc. Natl. Acad. Sci. USA* **2005**, *102*, 10451–10453.

[33] Radisavljevic, B.; Radenovic, A.; Brivio, J.; Giacometti, V.; Kis, A. Single-layer MoS_2 transistors. *Nat. Nanotechnol.* **2011**, *6*, 147–150.

[34] Fang, H.; Chuang, S.; Chang, T. C.; Takei, K.; Takahashi, T.; Javey, A. High-performance single layered WSe_2 p-FETs with chemically doped contacts. *Nano Lett.* **2012**, *12*, 3788–3792.

[35] Dean, C. R.; Young, A. F.; Meric, I.; Lee, C.; Wang, L.; Sorgenfrei, S.; Watanabe, K.; Taniguchi, T.; Kim, P.; Shepard, K. L. et al. Boron nitride substrates for high-quality graphene electronics. *Nat. Nanotechnol.* **2010**, *5*, 722–726.

[36] Castellanos-Gomez, A.; Agraït, N.; Rubio-Bollinger, G. Optical identification of atomically thin dichalcogenide crystals. *Appl. Phys. Lett.* **2010**, *96*, 213116.

[37] Late, D. J.; Liu, B.; Matte, H. S. S.; Rao, C. N. R.; Dravid, V. P. Rapid characterization of ultrathin layers of chalcogenides on SiO_2/Si substrates. *Adv. Funct. Mater.* **2012**, *22*, 1894–1905.

[38] Benameur, M. M.; Radisavljevic, B.; Héron, J.; Sahoo, S.; Berger, H.; Kis, A. Visibility of dichalcogenide nanolayers. *Nanotechnology* **2011**, *22*, 125706.

[39] Castellanos-Gomez, A.; Barkelid, M.; Goossens, A. M.; Calado, V. E.; van der Zant, H. S. J.; Steele, G. A. Laser-thinning of MoS_2: On demand generation of a single-layer semiconductor. *Nano Lett.* **2012**, *12*, 3187–3192.

[40] Britnell, L.; Gorbachev, R. V.; Jalil, R.; Belle, B. D.; Schedin, F.; Mishchenko, A.; Georgiou, T.; Katsnelson, M. I.; Eaves, L.; Morozov, S. V. et al. Field-effect tunneling transistor based on vertical graphene heterostructures. *Science* **2012**, *335*, 947–950.

[41] Castellanos-Gomez, A.; Buscema, M.; Molenaar, R.; Singh, V.; Janssen, L.; van der Zant, H. S. J.; Steele, G. A. Deterministic transfer of two-dimensional materials by all-dry viscoelastic stamping. *2D Mater.* **2014**, *1*, 011002.

[42] Geim, A. K.; Grigorieva, I. V. Van der Waals heterostructures. *Nature* **2013**, *499*, 419–425.

[43] Roy, K.; Padmanabhan, M.; Goswami, S.; Sai, T. P.; Ramalingam, G.; Raghavan, S.; Ghosh, A. Graphene–MoS_2 hybrid structures for multifunctional photoresponsive memory devices. *Nat. Nanotechnol.* **2013**, *8*, 826–830.

[44] Tian, H.; Tan, Z.; Wu, C.; Wang, X. M.; Mohammad, M. A.; Xie, D.; Yang, Y.; Wang, J.; Li, L.-J.; Xu, J. et al. Novel field-effect schottky barrier transistors based on graphene–MoS_2 heterojunctions. *Sci. Rep.* **2014**, *4*, 5951.

[45] Britnell, L.; Ribeiro, R. M.; Eckmann, A.; Jalil, R.; Belle, B. D.; Mishchenko, A.; Kim, Y.-J.; Gorbachev, R. V.; Georgiou, T.; Morozov, S. V. et al. Strong light–matter interactions in heterostructures of atomically thin films. *Science* **2013**, *340*, 1311–1314.

[46] Lee, C.-H.; Lee, G.-H.; van der Zande, A. M.; Chen, W. C.; Li, Y. L.; Han, M. Y.; Cui, X.; Arefe, G.; Nuckolls, C.; Heinz, T. F. et al. Atomically thin p–n junctions with van der Waals heterointerfaces. *Nat. Nanotechnol.* **2014**, *9*, 676–681.

[47] Nicolosi, V.; Chhowalla, M.; Kanatzidis, M. G.; Strano, M. S.; Coleman, J. N. Liquid exfoliation of layered materials. *Science* **2013**, *340*, 1226419.

[48] Hernandez, Y.; Nicolosi, V.; Lotya, M.; Blighe, F. M.; Sun, Z. Y.; De, S.; McGovern, I. T.; Holland, B.; Byrne, M.; Gun'Ko, Y. K. et al. High-yield production of graphene by liquid-phase exfoliation of graphite. *Nat. Nanotechnol.* **2008**, *3*, 563–568.

[49] Coleman, J. N.; Lotya, M.; O'Neill, A.; Bergin, S. D.; King, P. J.; Khan, U.; Young, K.; Gaucher, A.; De, S.; Smith, R. J. et al. Two-dimensional nanosheets produced by liquid exfoliation of layered materials. *Science* **2011**, *331*, 568–571.

[50] Paton, K. R.; Varrla, E.; Backes, C.; Smith, R. J.; Khan, U.; O'Neill, A.; Boland, C.; Lotya, M.; Istrate, O. M.; King, P. et al. Scalable production of large quantities of defect-free few-layer graphene by shear exfoliation in liquids. *Nat. Mater.* **2014**, *13*, 624–630.

[51] Sahoo, R. R.; Biswas, S. K. Microtribology and friction-induced material transfer in layered MoS_2 nanoparticles sprayed on a steel surface. *Tribol. Lett.* **2010**, *37*, 313–326.

[52] Sun, X. M.; Luo, D. C.; Liu, J. F.; Evans, D. G. Monodisperse chemically modified graphene obtained by density gradient ultracentrifugal rate separation. *ACS Nano* **2010**, *4*, 3381–3389.

[53] Kang, J.; Seo, J.-W. T.; Alducin, D.; Ponce, A.; Yacaman, M. J.; Hersam, M. C. Thickness sorting of two-dimensional transition metal dichalcogenides via copolymer-assisted density gradient ultracentrifugation. *Nat. Commun.* **2014**, *5*, 5478.

[54] Backes, C.; Smith, R. J.; McEvoy, N.; Berner, N. C.; McCloskey, D.; Nerl, H. C.; O'Neill, A.; King, P. J.; Higgins,

T.; Hanlon, D. et al. Edge and confinement effects allow *in situ* measurement of size and thickness of liquid-exfoliated nanosheets. *Nat. Commun.* **2014**, *5*, 4576.

[55] Eda, G.; Yamaguchi, H.; Voiry, D.; Fujita, T.; Chen, M. W.; Chhowalla, M. Photoluminescence from chemically exfoliated MoS_2. *Nano Lett.* **2011**, *11*, 5111–5116.

[56] Lee, Y. H.; Zhang, X. Q.; Zhang, W. J.; Chang, M. T.; Lin, C. T.; Chang, K. D.; Yu, Y. C.; Wang, J. T. W.; Chang, C. S.; Li, L. J. et al. Synthesis of large-area MoS_2 atomic layers with chemical vapor deposition. *Adv. Mater.* **2012**, *24*, 2320–2325.

[57] Zhang, J.; Yu, H.; Chen, W.; Tian, X. Z.; Liu, D. H.; Cheng, M.; Xie, G. B.; Yang, W.; Yang, R.; Bai, X. D. et al. Scalable growth of high-quality polycrystalline MoS_2 monolayers on SiO_2 with tunable grain sizes. *ACS Nano* **2014**, *8*, 6024–6030.

[58] Lee, Y.-H.; Yu, L. L.; Wang, H.; Fang, W. J.; Ling, X.; Shi, Y. M.; Lin, C.-T.; Huang, J.-K.; Chang, M.-T.; Chang, C.-S. et al. Synthesis and transfer of single-layer transition metal disulfides on diverse surfaces. *Nano Lett.* **2013**, *13*, 1852–1857.

[59] Lin, Y.-C.; Zhang, W. J.; Huang, J.-K.; Liu, K.-K.; Lee, Y.-H.; Liang, C.-T.; Chu, C.-W.; Li, L.-J. Wafer-scale MoS_2 thin layers prepared by MoO_3 sulfurization. *Nanoscale* **2012**, *4*, 6637–6641.

[60] Wang, H.; Yu, L. L.; Lee, Y.-H.; Shi, Y. M.; Hsu, A.; Chin, M. L.; Li, L.-J.; Dubey, M.; Kong, J.; Palacios, T. Integrated circuits based on bilayer MoS_2 transistors. *Nano Lett.* **2012**, *12*, 4674–4680.

[61] Wang, H.; Yu, L.; Lee, Y.-H.; Fang, W.; Hsu, A.; Herring, P.; Chin, M.; Dubey, M.; Li, L.-J.; Kong, J. et al. Large-scale 2D electronics based on single-layer MoS_2 grown by chemical vapor deposition. In *Proceedings of the 2012 IEEE International Electron Device Meeting (IEDM)*, San Francisco, USA, 2012, pp 4.6.1–4.6.4.

[62] Liu, K.-K.; Zhang, W. J.; Lee, Y.-H.; Lin, Y.-C.; Chang, M.-T.; Su, C.-Y.; Chang, C.-S.; Li, H.; Shi, Y. M.; Zhang, H. et al. Growth of large-area and highly crystalline MoS_2 thin layers on insulating substrates. *Nano Lett.* **2012**, *12*, 1538–1544.

[63] van der Zande, A. M.; Huang, P. Y.; Chenet, D. A.; Berkelbach, T. C.; You, Y.; Lee, G.-H.; Heinz, T. F.; Reichman, D. R.; Muller, D. A.; Hone, J. C. Grains and grain boundaries in highly crystalline monolayer molybdenum disulphide. *Nat. Mater.* **2013**, *12*, 554–561.

[64] Najmaei, S.; Liu, Z.; Zhou, W.; Zou, X. L.; Shi, G.; Lei, S. D.; Yakobson, B. I.; Idrobo, J.-C.; Ajayan, P. M.; Lou, J. Vapour phase growth and grain boundary structure of molybdenum disulphide atomic layers. *Nat. Mater.* **2013**, *12*, 754–759.

[65] Kang, K.; Xie, S.; Huang, L. J.; Han, Y. M.; Huang, P. Y.; Mak, K. F.; Kim, C.-J.; Muller, D.; Park, J. High-mobility three-atom-thick semiconducting films with wafer-scale homogeneity. *Nature* **2015**, *520*, 656–660.

[66] Marks, T. J.; Hersam, M. C. Materials science: Semiconductors grown large and thin. *Nature* **2015**, *520*, 631–632.

[67] Huang, C. M.; Wu, S. F.; Sanchez, A. M.; Peters, J. J. P.; Beanland, R.; Ross, J. S.; Rivera, P.; Yao, W.; Cobden, D. H.; Xu, X. D. Lateral heterojunctions within monolayer $MoSe_2$–WSe_2 semiconductors. *Nat. Mater.* **2014**, *13*, 1096–1101.

[68] Yu, Y. F.; Hu, S.; Su, L. Q.; Huang, L. J.; Liu, Y.; Jin, Z. H.; Purezky, A. A.; Geohegan, D. B.; Kim, K. W.; Zhang, Y. et al. Equally efficient interlayer exciton relaxation and improved absorption in epitaxial and nonepitaxial MoS_2/WS_2 heterostructures. *Nano Lett.* **2015**, *15*, 486–491.

[69] Gong, Y. J.; Lin, J. H.; Wang, X. L.; Shi, G.; Lei, S. D.; Lin, Z.; Zou, X. L.; Ye, G. L.; Vajtai, R.; Yakobson, B. I. et al. Vertical and in-plane heterostructures from WS_2/MoS_2 monolayers. *Nat. Mater.* **2014**, *13*, 1135–1142.

[70] Chen, K.; Wan, X.; Xie, W. G.; Wen, J. X.; Kang, Z. W.; Zeng, X. L.; Chen, H. J.; Xu, J. B. Lateral built-in potential of monolayer MoS_2–WS_2 in-plane heterostructures by a shortcut growth strategy. *Adv. Mater.* **2015**, *27*, 6431–6437.

[71] Duan, X. D.; Wang, C.; Shaw, J. C.; Cheng, R.; Chen, Y.; Li, H. L.; Wu, X. P.; Tang, Y.; Zhang, Q. L.; Pan, A. L. et al. Lateral epitaxial growth of two-dimensional layered semiconductor heterojunctions. *Nat. Nanotechnol.* **2014**, *9*, 1024–1030.

[72] Li, M.-Y.; Shi, Y.; Cheng, C.-C.; Lu, L.-S.; Lin, Y.-C.; Tang, H.-L.; Tsai, M.-L.; Chu, C.-W.; Wei, K.-H.; He, J.-H. et al. Epitaxial growth of a monolayer WSe_2–MoS_2 lateral p–n junction with an atomically sharp interface. *Science* **2015**, *349*, 524–528.

[73] Gong, Y. J.; Lei, S. D.; Ye, G. L.; Li, B.; He, Y. M.; Keyshar, K.; Zhang, X.; Wang, Q. Z.; Lou, J.; Liu, Z. et al. Two-step growth of two-dimensional WSe_2/$MoSe_2$ heterostructures. *Nano Lett.* **2015**, *15*, 6135–6141.

[74] Chen, K.; Wan, X.; Wen, J. X.; Xie, W. G.; Kang, Z. W.; Zeng, X. L.; Chen, H. J.; Xu, J.-B. Electronic properties of MoS_2–WS_2 heterostructures synthesized with two-step lateral epitaxial strategy. *ACS Nano* **2015**, *9*, 9868–9876.

[75] Zhang, Q.; Xiao, X.; Zhao, R. Q.; Lv, D. H.; Xu, G. C.; Lu, Z. X.; Sun, L. F.; Lin, S. Z.; Gao, X.; Zhou, J. et al. Two-dimensional layered heterostructures synthesized from core-shell nanowires. *Angew. Chem., Int. Ed.* **2015**, *54*, 8957–8960.

[76] Yin, Z. Y.; Li, H.; Li, H.; Jiang, L.; Shi, Y. M.; Sun, Y. H.; Lu, G.; Zhang, Q.; Chen, X. D.; Zhang, H. Single-layer MoS_2 phototransistors. *ACS Nano* **2012**, *6*, 74–80.

[77] Choi, W.; Cho, M. Y.; Konar, A.; Lee, J. H.; Cha, G. B.; Hong, S. C.; Kim, S.; Kim, J.; Jena, D.; Joo, J. et al. High-detectivity multilayer MoS_2 phototransistors with spectral response from ultraviolet to infrared. *Adv. Mater.* **2012**, *24*, 5832–5836.

[78] Lopez-Sanchez, O.; Lembke, D.; Kayci, M.; Radenovic, A.; Kis, A. Ultrasensitive photodetectors based on monolayer MoS_2. *Nat. Nanotechnol.* **2013**, *8*, 497–501.

[79] Furchi, M. M.; Polyushkin, D. K.; Pospischil, A.; Mueller, T. Mechanisms of photoconductivity in atomically thin MoS_2. *Nano Lett.* **2014**, *14*, 6165–6170.

[80] Huo, N. J.; Yang, S. X.; Wei, Z. M.; Li, S.-S.; Xia, J.-B.; Li, J. B. Photoresponsive and gas sensing field-effect transistors based on multilayer WS_2 nanoflakes. *Sci. Rep.* **2014**, *4*, 5209.

[81] Yang, S. X.; Tongay, S.; Yue, Q.; Li, Y. T.; Li, B.; Lu, F. Y. High-performance few-layer Mo-doped $ReSe_2$ nanosheet photodetectors. *Sci. Rep.* **2014**, *4*, 5442.

[82] Yu, W. J.; Liu, Y.; Zhou, H. L.; Yin, A. X.; Li, Z.; Huang, Y.; Duan, X. F. Highly efficient gate-tunable photocurrent generation in vertical heterostructures of layered materials. *Nat. Nanotechnol.* **2013**, *8*, 952–958.

[83] Zhang, W. J.; Chuu, C.-P.; Huang, J.-K.; Chen, C.-H.; Tsai, M.-L.; Chang, Y.-H.; Liang, C.-T.; Chen, Y.-Z.; Chueh, Y.-L.; He, J.-H. et al. Ultrahigh-gain photodetectors based on atomically thin graphene–MoS_2 heterostructures. *Sci. Rep.* **2014**, *4*, 3826.

[84] Jariwala, D.; Sangwan, V. K.; Wu, C.-C.; Prabhumirashi, P. L.; Geier, M. L.; Marks, T. J.; Lauhon, L. J.; Hersam, M. C. Gate-tunable carbon nanotube–MoS_2 heterojunction p–n diode. *Proc. Natl. Acad. Sci. USA* **2013**, *110*, 18076–18080.

[85] Lin, J. D.; Li, H.; Zhang, H.; Chen, W. Plasmonic enhancement of photocurrent in MoS_2 field-effect-transistor. *Appl. Phys. Lett.* **2013**, *102*, 203109.

[86] Sobhani, A.; Lauchner, A.; Najmaei, S.; Ayala-Orozco, C.; Wen, F. F.; Lou, J.; Halas, N. J. Enhancing the photocurrent and photoluminescence of single crystal monolayer MoS_2 with resonant plasmonic nanoshells. *Appl. Phys. Lett.* **2014**, *104*, 031112.

[87] Kang, Y. M.; Najmaei, S.; Liu, Z.; Bao, Y. J.; Wang, Y. M.; Zhu, X.; Halas, N. J.; Nordlander, P.; Ajayan, P. M.; Lou, J. et al. Plasmonic hot electron induced structural phase transition in a MoS_2 monolayer. *Adv. Mater.* **2014**, *26*, 6467–6471.

[88] Akselrod, G. M.; Ming, T.; Argyropoulos, C.; Hoang, T. B.; Lin, Y. X.; Ling, X.; Smith, D. R.; Kong, J.; Mikkelsen, M. H. Leveraging nanocavity harmonics for control of optical processes in 2D semiconductors. *Nano Lett.* **2015**, *15*, 3578–3584.

[89] Lee, J.; Hernandez, P.; Lee, J.; Govorov, A. O.; Kotov, N. A. Exciton–plasmon interactions in molecular spring assemblies of nanowires and wavelength-based protein detection. *Nat. Mater.* **2007**, *6*, 291–295.

[90] Najmaei, S.; Mlayah, A.; Arbouet, A.; Girard, C.; Léotin, J.; Lou, J. Plasmonic pumping of excitonic photoluminescence in hybrid MoS_2–Au nanostructures. *ACS Nano* **2014**, *8*, 12682–12689.

[91] Sundaram, R. S.; Engel, M.; Lombardo, A.; Krupke, R.; Ferrari, A. C.; Avouris, P.; Steiner, M. Electroluminescence in single layer MoS_2. *Nano Lett.* **2013**, *13*, 1416–1421.

[92] Pospischil, A.; Furchi, M. M.; Mueller, T. Solar-energy conversion and light emission in an atomic monolayer p–n diode. *Nat. Nanotechnol.* **2014**, *9*, 257–261.

[93] Ross, J. S.; Klement, P.; Jones, A. M.; Ghimire, N. J.; Yan, J. Q.; Mandrus, D. G.; Taniguchi, T.; Watanabe, K.; Kitamura, K.; Yao, W. et al. Electrically tunable excitonic light-emitting diodes based on monolayer WSe_2 p–n junctions. *Nat. Nanotechnol.* **2014**, *9*, 268–272.

[94] Baugher, B. W.; Churchill, H. O.; Yang, Y. F.; Jarillo-Herrero, P. Optoelectronic devices based on electrically tunable p–n diodes in a monolayer dichalcogenide. *Nat. Nanotechnol.* **2014**, *9*, 262–267.

[95] Zhang, Y. J.; Oka, T.; Suzuki, R.; Ye, J. T.; Iwasa, Y. Electrically switchable chiral light-emitting transistor. *Science* **2014**, *344*, 725–728.

[96] Lopez-Sanchez, O.; Alarcon Llado, E.; Koman, V.; Fontcuberta i Morral, A.; Radenovic, A.; Kis, A. Light generation and harvesting in a van der Waals heterostructure. *ACS Nano* **2014**, *8*, 3042–3048.

[97] Cheng, R.; Li, D. H.; Zhou, H. L.; Wang, C.; Yin, A. X.; Jiang, S.; Liu, Y.; Chen, Y.; Huang, Y.; Duan, X. F. Electroluminescence and photocurrent generation from atomically sharp WSe_2/MoS_2 heterojunction p–n diodes. *Nano Lett.* **2014**, *14*, 5590–5597.

[98] Withers, F.; Del Pozo-Zamudio, O.; Mishchenko, A.; Rooney, A. P.; Gholinia, A.; Watanabe, K.; Taniguchi, T.; Haigh, S. J.; Geim, A. K.; Tartakovskii, A. I. et al. Light-emitting diodes by band-structure engineering in van der Waals heterostructures. *Nat. Mater.* **2015**, *14*, 301–306.

[99] Wu, S. F.; Buckley, S.; Schaibley, J. R.; Feng, L. F.; Yan, J. Q.; Mandrus, D. G.; Hatami, F.; Yao, W.; Vučković, J.; Majumdar, A. et al. Monolayer semiconductor nanocavity lasers with ultralow thresholds. *Nature* **2015**, *520*, 69–72.

[100] Ye, Y.; Wong, Z. J.; Lu, X. F.; Ni, X. J.; Zhu, H. Y.; Chen, X. H.; Wang, Y.; Zhang, X. Monolayer excitonic laser. *Nat. Photon.* **2015**, *9*, 733–737.

[101] Salehzadeh, O.; Djavid, M.; Tran, N. H.; Shih, I.; Mi, Z. T. Optically pumped two-dimensional MoS_2 lasers operating

at room-temperature. *Nano Lett.* **2015**, *15*, 5302–5306.

[102] Mak, K. F.; Lee, C.; Hone, J.; Shan, J.; Heinz, T. F. Atomically thin MoS_2: A new direct-gap semiconductor. *Phys. Rev. Lett.* **2010**, *105*, 136805.

[103] Mak, K. F.; He, K. L.; Shan, J.; Heinz, T. F. Control of valley polarization in monolayer MoS_2 by optical helicity. *Nat. Nanotechnol.* **2012**, *7*, 494–498.

[104] Splendiani, A.; Sun, L.; Zhang, Y. B.; Li, T. S.; Kim, J.; Chim, C.-Y.; Galli, G.; Wang, F. Emerging photoluminescence in monolayer MoS_2. *Nano Lett.* **2010**, *10*, 1271–1275.

[105] Li, T. Y.; Liu, Y.-H.; Porter, S.; Goldberger, J. E. Dimensionally reduced one-dimensional chains of $TiSe_2$. *Chem. Mater.* **2013**, *25*, 1477–1479.

[106] Friend, R. H.; Jerome, D.; Liang, W. Y.; Mikkelsen, C.; Yoffe, A. D. Semimetallic character of $TiSe_2$ and semiconductor character of TiS_2 under pressure. *J. Phys. C: Solid State Phys.* **1977**, *10*, L705.

[107] Chen, C. H.; Fabian, W.; Brown, F. C.; Woo, K. C.; Davies, B.; DeLong, B.; Thompson, A. H. Angle-resolved photoemission studies of the band structure of $TiSe_2$ and TiS_2. *Phys. Rev. B* **1980**, *21*, 615.

[108] Traving, M.; Seydel, T.; Kipp, L.; Skibowski, M.; Starrost, F.; Krasovskii, E. E.; Perlov, A.; Schattke, W. Combined photoemission and inverse photoemission study of HfS_2. *Phys. Rev. B* **2001**, *63*, 035107.

[109] Mattheiss, L. F. Band structures of transition-metal-dichalcogenide layer compounds. *Phys. Rev. B* **1973**, *8*, 3719–3740.

[110] Georgiou, T.; Jalil, R.; Belle, B. D.; Britnell, L.; Gorbachev, R. V.; Morozov, S. V.; Kim, Y.-J.; Gholinia, A.; Haigh, S. J.; Makarovsky, O. et al. Vertical field-effect transistor based on graphene–WS_2 heterostructures for flexible and transparent electronics. *Nat. Nanotechnol.* **2013**, *8*, 100–103.

[111] Furchi, M. M.; Pospischil, A.; Libisch, F.; Burgdörfer, J.; Mueller, T. Photovoltaic effect in an electrically tunable van der Waals heterojunction. *Nano Lett.* **2014**, *14*, 4785–4791.

[112] Buscema, M.; Groenendijk, D. J.; Steele, G. A.; van der Zant, H. S. J.; Castellanos-Gomez, A. Photovoltaic effect in few-layer black phosphorus PN junctions defined by local electrostatic gating. *Nat. Commun.* **2014**, *5*, 4651.

[113] Xia, F. N.; Wang, H.; Jia, Y. C. Rediscovering black phosphorus as an anisotropic layered material for optoelectronics and electronics. *Nat. Commun.* **2014**, *5*, 4458.

[114] Xia, F. N.; Wang, H.; Xiao, D.; Dubey, M.; Ramasubramaniam, A. Two-dimensional material nanophotonics. *Nat. Photon.* **2014**, *8*, 899–907.

[115] Ling, X.; Wang, H.; Huang, S. X.; Xia, F. N.; Dresselhaus, M. S. The renaissance of black phosphorus. *Proc. Natl. Acad. Sci. USA* **2015**, *112*, 4523–4530.

[116] Wang, X. M.; Jones, A. M.; Seyler, K. L.; Tran, V.; Jia, Y. C.; Zhao, H.; Wang, H.; Yang, L.; Xu, X. D.; Xia, F. N. Highly anisotropic and robust excitons in monolayer black phosphorus. *Nat. Nanotechnol.* **2015**, *10*, 517–521.

[117] Yuan, H. T.; Liu, X. G.; Afshinmanesh, F.; Li, W.; Xu, G.; Sun, J.; Lian, B.; Curto, A. G.; Ye, G. J.; Hikita, Y. et al. Polarization-sensitive broadband photodetector using a black phosphorus vertical p–n junction. *Nat. Nanotechnol.* **2015**, *10*, 707–713.

[118] Xiao, D.; Liu, G.-B.; Feng, W. X.; Xu, X. D.; Yao, W. Coupled spin and valley physics in monolayers of MoS_2 and other group-VI dichalcogenides. *Phys. Rev. Lett.* **2012**, *108*, 196802.

[119] Zeng, H. L.; Dai, J. F.; Yao, W.; Xiao, D.; Cui, X. D. Valley polarization in MoS_2 monolayers by optical pumping. *Nat. Nanotechnol.* **2012**, *7*, 490–493.

[120] Jones, A. M.; Yu, H. Y.; Ghimire, N. J.; Wu, S. F.; Aivazian, G.; Ross, J. S.; Zhao, B.; Yan, J. Q.; Mandrus, D. G.; Xiao, D. et al. Optical generation of excitonic valley coherence in monolayer WSe_2. *Nat. Nanotechnol.* **2013**, *8*, 634–638.

[121] Yuan, H. T.; Wang, X. Q.; Lian, B.; Zhang, H. J.; Fang, X. F.; Shen, B.; Xu, G.; Xu, Y.; Zhang, S.-C.; Hwang, H. Y. et al. Generation and electric control of spin–valley-coupled circular photogalvanic current in WSe_2. *Nat. Nanotechnol.* **2014**, *9*, 851–857.

[122] Wang, X. M.; Xia, F. N. Van der Waals heterostructures: Stacked 2D materials shed light. *Nat. Mater.* **2015**, *14*, 264–265.